available at www.sciencedirect.com

ScienceDirect

journal homepage: www.elsevier.com/locate/chnjc

Article

Polycondensation of ammonium thiocyanate into novel porous g-C_3N_4 nanosheets as photocatalysts for enhanced hydrogen evolution under visible light irradiation

Yanjuan Cui *, Yuxiong Wang, Hao Wang, Fu Cao, Fangyan Chen

School of Environmental and Chemical Engineering, Jiangsu University of Science and Technology, Zhenjiang 212003, Jiangsu, China

ARTICLE INFO

Article history:
Received 11 May 2016
Accepted 18 July 2016
Published 5 November 2016

Keywords:
Carbon nitride
Nanosheet
Semiconductor
Ammonia
Photocatalysis
Hydrogen evolution

ABSTRACT

Porous graphitic carbon nitride (pg-C_3N_4) nanosheets have been prepared through a one-step ammonia thermopolymerization method. The effects of synthetic temperature on the structural, optical and photocatalytic properties of the samples have been investigated. Characterization results show that the heptazine-based conjugate heterocyclic structure was formed over 500 °C, which is attributed to the inhibitory effect of ammonia from the decomposition of NH_4SCN. Precise nanosheet morphology and an increased pore distribution with an enlarged surface area are observed for the samples obtained under high temperatures. Optical analysis results show that the bandgap of the samples widens and photoluminescene intensity is gradually quenched as the treating temperature is increased. The results demonstrate that a higher polymerization temperature improves the nanolayer structure, porosity and migration rate of the photo-induced carriers of the samples. The pg-C_3N_4 nanosheets prepared at 600 °C presents the highest photocatalytic activity for hydrogen evolution from water under visible-light irradiation. This study demonstrates a novel strategy for the synthesis and optimization of polymer semiconductor nanosheets with gratifying photocatalytic performance.

1. Introduction

Two-dimensional (2D) graphene-analogue semiconductor materials, based on the typical layer structured semiconductors, exhibit peculiar and fascinating properties in contrast with those of their bulk parent compounds [1]. The exceptional properties of 2D semiconductors, such as piezoelectric coupling and band energy transition, will enable new breakthroughs in nanomaterials science [2,3]. Inevitably, the photochemistry of 2D semiconductor photocatalysts has received increasing attention to address the problem of the usage of solar energy. Previous studies have reported the fabrication of semiconductors into 2D nanosheets for photocatalytic application, such as layered MoS_2, WS_2, SnS_2, TiO_2 and so forth [4–7]. Theoretical analysis has shown that 2D graphene-analogue materials possess many advantages as catalysts in a visible-light photocatalytic reaction, such as increasing the absorption of light, surface area, speed of carrier transport and so forth.

Recently, 2D metal-free materials, as key determinants of cost-effective hydrogen generation on a large-scale, have been identified as newcomers to the family of photocatalysts [8].

* Corresponding author. Tel/Fax: +86-511-85605157; E-mail: yjcui@just.edu.cn
The work was supported by the National Natural Science Foundation of China (21503096) and the Natural Science Foundation of Jiangsu Province (BK20140507).
DOI: 10.1016/S1872-2067(16)62509-3 | http://www.sciencedirect.com/science/journal/18722067 | Chin. J. Catal., Vol. 37, No. 11, November 2016

Graphitic carbon nitride (g-C_3N_4), a sustainable conjugated 2D polymer semiconductor with a medium band gap of 2.7 eV, has been shown to exhibit great potential to scientists searching for new materials for energy conversion in the future [9–11]. As is desired for analogues of graphene, g-C_3N_4 possesses a graphitic-like layered structure and involves van der Waals interactions between adjacent C–N layers with strong covalent bonding between each layer. Therefore, its 2D layers present promising opto-electronic properties and facilitate coupling with various functional materials to enhance the performance [12–14]. However, the preparation of their nanosheet structures with atomic scale thickness remains difficult owing to the experimental challenges.

Motivated by the intriguing graphene chemistry, the exfoliation of bulk g-C_3N_4 into single- or few layer-2D layers has been actively pursued. Mechanical liquid ultrasonication-assisted exfoliation in water and organic solvents, such as ethanol and isopropanol, has been used to achieve g-C_3N_4 nanosheets [15,16]. The chemical oxidation etching method has generally been regarded as an efficient preparation method for 2D g-C_3N_4 nanosheets with a unilamellar structure. With the progress in this field, oxidant HNO_3 or H_2SO_4 have been used as intercalation compounds [17,18], and other intercalation compounds have also been reported recently [19,20]. However, the obtained catalysts were often doped materials. For example, Song *et al*. [21] obtained few-layer-thick g-C_3N_4 nanosheets from liquid ammonia (LA)-assisted lithiation, and the samples showed an enhanced photocatalytic redox activity with respect to both photocatalytic H_2 evolution and hydroxyl radical generation. Dong *et al*. [22] prepared a stable colloidal suspension of g-C_3N_4 nanosheets through an H_2SO_4 exfoliation route. Recently, Zhang *et al*. [23] reported a one-step electrochemical method to prepare ultrathin g-C_3N_4 nanosheets from melamine and the as-synthesized materials showed intrinsic peroxidase-like activity. However, structure disorder was observed owing to the partial destruction of the triazine units under the electrolytic process. Thus, developing a facile method for the large-scale production of well-dispersed g-C_3N_4 nanosheets is urgently required. The approach of thermal oxidation exfoliation is regarded as highly efficient and environmentally friendly [24]. Currently, the most direct and simple method to prepare g-C_3N_4 composed with nanosheet-like morphology is direct pyrocondensation of urea or thiourea [25]. Nevertheless, its microstructure and ability for photocatalytic hydrogen evolution still needs optimization [26].

The introduction of nanopores into the bulk structure of g-C_3N_4 could effectively increase the specific surface area, thereby increasing the number of surface active sites and photocatalytic activities of the catalysts. A number of methods have been discussed for the preparation of porous g-C_3N_4, including replicating the synthesis from SiO_2 templates or soft templates [27–29], using pore-forming agents [30], and protonation processes [31]. However, during the synthetic progress, the compellent pore-creation leads to incomplete condensation of carbon nitride and increases the disorder of the layer stacking structure. Hence, this becomes unfavorable to the improvement of electron transmission and photocatalytic performance. Therefore, a direct route for 2D g-C_3N_4 nanosheets with high polymerization degree and porosity needs to be developed to further improve the photocatalytic activity. Recently, ammonia thermopolymerization was developed by our group to prepare g-C_3N_4 with a high degree of condensation polymerization [32]. Based on this method, porous g-C_3N_4 nanosheets are expected to be achieved by a one-step process.

In this work, porous g-C_3N_4 nanosheets were synthesized by the direct ammonia thermopolymerization method at different temperatures. Experimental results confirmed that a higher condensation temperature increases the surface area and pore structure, optimizes the photoelectric properties of catalysts to inhibit the recombination of carriers, and therefore, enhances the photocatalytic activity for the H_2 evolution under visible-light irradiation.

2. Experimental

2.1. Catalyst preparation

All materials were purchased from Sinopharm Chemical Reagent Co., Ltd. (Shanghai, China) and used as received without further purification.

Porous g-C_3N_4 nanosheet photocatalysts (pg-C_3N_4) were prepared using the ammonia-polymerization approach [32]. In a typical procedure, 10 g of ammonium thiocyanate (NH_4SCN) was placed in a tube furnace and then heated to a certain temperature in the range of 450–600 °C for 2 h with a ramp rate of 5 °C/min in an ammonia atmosphere, followed by naturally cooling to room temperature. Air was removed for 30 min through ammonia before heating. Final products were obtained after grinding the products into powders and were denoted as CN-*T*, where *T* refers to the calcination temperature (°C).

2.2. Catalyst characterization

X-ray diffraction (XRD) patterns were collected on a Bruker D8 Advance diffractometer with Cu K_α radiation (λ = 1.5406 Å). Fourier transformed infrared (FTIR) spectra were obtained using a Nicolet Magna 670 FTIR spectrometer in KBr at a concentration of approximately 1 wt%. Nitrogen adsorption-desorption isotherms were collected at –196 °C using a Micromeritics ASAP 2020 surface area and porosity analyzer. Ultraviolet-visible (UV-vis) diffuse reflectance spectroscopy (DRS) was performed on a Varian Cary 500 Scan UV-visible system. Scanning electron microscopy (SEM) was performed using a JEOL model JSM-6700F instrument. The photoluminescence (PL) emission spectra were recorded on an Edinburgh FI/FSTCSPC 920 fluorescence spectrometer. Electron paramagnetic resonance (EPR) measurements were carried out on a Bruker model A300 spectrometer.

2.3. Photocatalytic study

Photocatalytic activity was evaluated by the photocatalytic

hydrogen evolution from water under visible light irradiation (λ > 420 nm). Reactions were carried out in a Pyrex top-irradiation reaction vessel connected to a glass closed gas system. In each experiment, 50 mg of photocatalyst powder was dispersed in an aqueous solution (100 mL) containing triethanolamine (10 vol%) as a sacrificial electron donor. Pt (3 wt%) was loaded on the surface of the catalyst by in situ photodeposition using H_2PtCl_6. The reaction solution was evacuated several times to completely remove air prior to irradiation under a 300-W xenon lamp. The wavelength of the incident light was controlled by applying the appropriate cut-off filters. The temperature of the reaction solution was maintained at room temperature by the flow of cooling water during the reaction. The evolved gases were analyzed by gas chromatography equipped with a thermal conductivity detector (TCD) and a 5-Å molecular sieve column, using argon as the carrier gas.

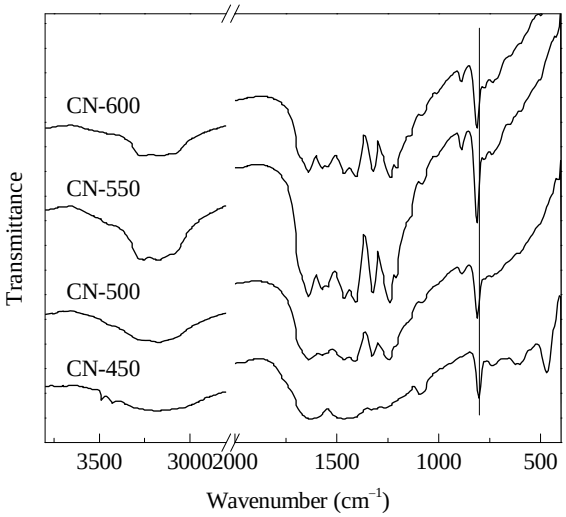

Fig. 2. FTIR spectra of samples obtained at different temperatures.

3. Results and discussion

3.1. Structure characterization

Fig. 1 exhibits the XRD patterns of the g-C_3N_4 samples condensed at different heating temperatures in ammonia. It can be observed at 450 °C, graphitic-like networks are incompletely formed. Upon increasing the calcination temperature to 500 °C, the distinctive graphitic-like structure (JPCDS 87-1526) is evolved. The strong diffraction peaks at approximately 27.5° and 13.0° are indexed as (002) of the inter-layer stacking reflection and (100) of the in-plane structure repeating motif of heptazine-based g-CN, respectively. Obviously, the polymerization temperature was increased compared with our previous work in which a graphitic C_3N_4 structure could be formed at 450 °C with NH_4SCN heating in nitrogen. This may be attributed to the inhibitory effect of deamination of NH_4SCN in extra ammonia, which is beneficial for the condensation degree of NH_4SCN to g-C_3N_4.

For CN-500, CN-550 and CN-600, with a heating temperature increase, the intensities of the XRD peaks are not weakened and become narrower, indicating an optimized polycondensation of g-C_3N_4. Compared with previous reports that a higher temperature usually induces decomposition of the g-C_3N_4, a highly condensed and compact packing of the conjugated skeleton of g-C_3N_4 could be achieved during ammonia polymerization. In addition, the (002) peak displays an up-shift from 27.5° to 27.8°, corresponding to a reduction in the stacking distance from 0.324 to 0.320 nm of the graphitic layer. Hence, a denser layer packing structure was achieved at a higher condensation temperature. Considering the pronounced peak at approximately 13.0°, no obvious difference could be detected among the CN-500 to CN-600 samples. This indicates that the three samples possess virtually the same void-to-void distance (d = 0.681 nm) of the in-plane structural repeating motifs, and the in-plane connection structure of the samples is well maintained even if synthesized at 600 °C.

FTIR spectra of CN synthesized at different temperatures in ammonia are shown in Fig. 2. Clearly, for the sample synthesized at 450 °C, the weak bands in the 1200–1700 cm^{-1} range and at 810 cm^{-1} are attributable to the organic molecules containing s-triazine ring moieties. However, the strong peak near 480 cm^{-1}, corresponding to C–S vibration, also exist, which

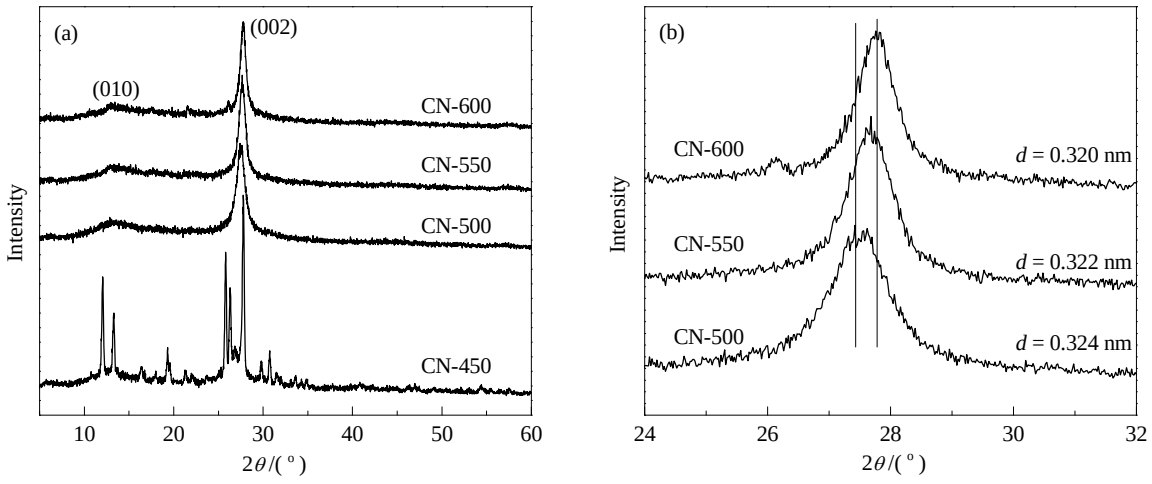

Fig. 1. XRD patterns of samples.

illustrates the incomplete condensation of the g-C_3N_4 samples.

When the temperature exceeds 500 °C, a practically complete desulphurization takes place and the as-prepared samples show typical IR peaks of C_3N_4. The bands at 1200–1700 cm^{-1} (1640, 1468, 1320, 1238 cm^{-1}) are regarded as stretching vibration peaks of the thiazine or heptazine heterocyclic ring (C_6N_7) units and broad absorption in the region of 3100–3300 cm^{-1} is related to the stretching modes of residual secondary and primary amines or absorbed water. For CN-500 to CN-600, the slight shift (4 cm^{-1}) to a higher wavenumber of the sharp peak at ~810 cm^{-1}, which is considered as a characteristic breathing mode of C_6N_7 units, illustrates the improved conjugation of the tri-s-triazine structure [33]. The small change of all these bands indicates that the porous carbon nitride nanosheets obtained at different heat-treatment temperatures does not lead to notable changes in the basic unit of CN samples. These IR spectra clearly prove that NH_4SCN can undergo condensation processes to construct a heterocyclic tri-s-triazine ring system in ammonia, and higher temperatures enable the obtained samples to possess a higher content of the tri-s-triazine phase.

The textural properties of CN-*T* samples were analyzed using a nitrogen adsorption-desorption spectrometer. The isotherms and the Barrett-Joyner-Halenda (BJH) pore size distributions are shown in Fig. 3. The isotherms of the samples show typical hysteresis, proving the existence of mesopores connected by micropores. The Brunauer-Emmett-Teller (BET) surface area (A_{BET}), BJH pore sizes, and pore volumes are summarized in Table 1. The A_{BET} and nanopores of CN-*T* were shown to be closely dependent on the calcination temperature. For CN-450, the A_{BET} was only 9 m^2/g, with the equivalent bulk CN catalyst prepared from NH_4SCN in nitrogen. When increasing the heating temperature from 500 to 600 °C, the A_{BET} of CN-*T* increased from 20 to 52 m^2/g. The average pore diameter and pore volume of the samples also increased with an increased calcination temperature. Interestingly, for the CN-500 to CN-600 samples, in addition to the enlarged mesopore volume, micropore sizes centered at approximately 3.8 nm appeared and these pore volumes also increased. The enlarged surface area and increased pore volumes could increase the surface mass transfer and improve the light absorption by reducing the light scattering, therefore enhancing the photocatalytic performance.

Table 1
Physicochemical properties and photocatalytic activity of CN-T for H_2 evolution with visible light.

Catalyst	A_{BET} [a] (m^2/g)	Pore volume (cm^3/g)	Pore size (nm)	Bang gap (eV)	H_2 evolution rate (μmol/h)
CN-450	9	0.03	24.5	2.62	87
CN-500	20	0.25	2.87	2.74	152
CN-550	46	0.25	20.5	2.86	304
CN-600	52	0.26	18.8	2.92	340

[a] Specific surface area.

In this work, the grain morphology of CN-*T* catalysts obtained under different temperatures was investigated by SEM analysis, and clear pictures are shown in Fig. 4. It is evident that the CN-500 sample presents an irregular bulk stacking like the intrinsic samples prepared in nitrogen. With an increasing temperature, smaller particles and a sheet structure distribution could be observed for CN-550. Furthermore, a remarkable nanosheet morphology accompanied with nanopores was apparent for CN-600. The results are consistent with the increased surface area and nanopores of these samples. The formation of the 2D nanosheet structure is an important factor to improve the photocatalytic performance. Meanwhile, the formation of nanopores in a graphitic layer of g-C_3N_4 is predictable for the improvement of the photocatalytic activity.

The optical features of the as-prepared CN-*T* materials were examined by UV-vis DRS, as shown in Fig. 5. All samples demonstrated semiconductor-like absorptions in the blue visible light range. As expected, increasing the heating temperature from 400 to 600 °C, the absorption edges of products showed a hypochromatic shift from 452 to 424 nm, corresponding to E_g = 2.74 to 2.92 eV for CN-500 to CN-600, owing to the strong quantum size confinement effect. Although a decreased optical absorption in the visible light region was generated, the formation of a layer structure, which was compressed to a smaller inter-plane distance, together with the enlarged surface area

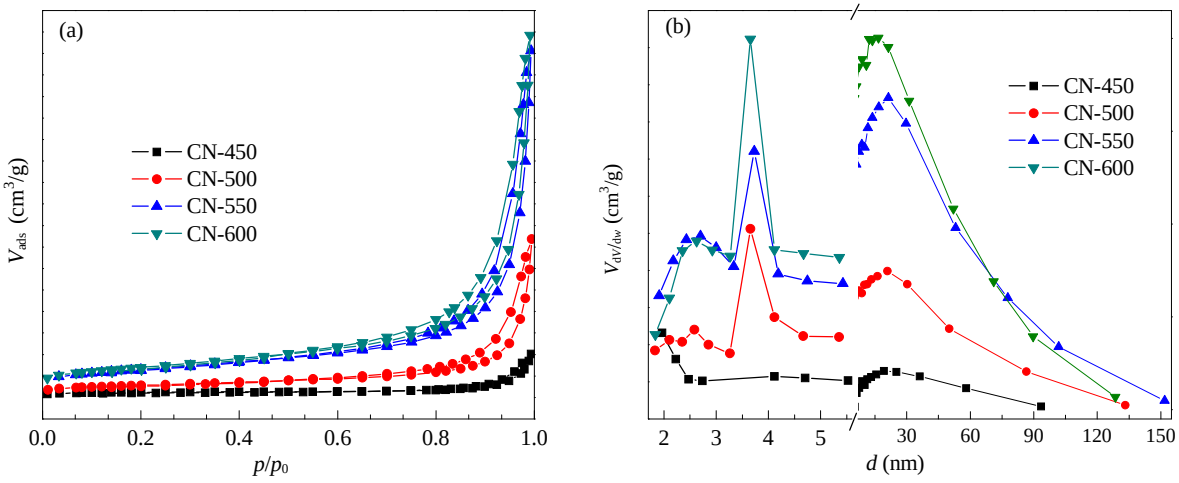

Fig. 3. N_2 adsorption-desorption isotherms (a) and the corresponding BJH pore-size distribution (b) of different samples.

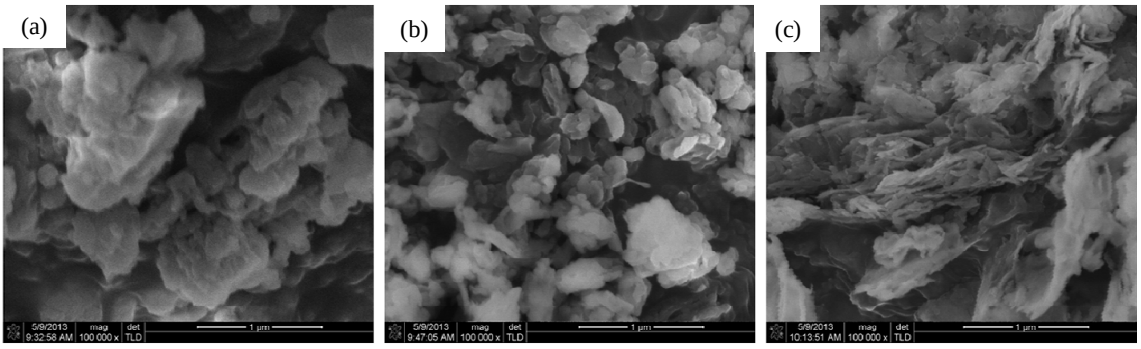

Fig. 4. Typical SEM micrographs of CN-500 (a), CN-550 (b) and CN-600 (c) samples.

are believed to promote the photocatalytic redox functions.

Room-temperature PL spectra were obtained using excitation light of 400 nm to investigate the efficiency of charge-carrier separation/recombination in the materials. As shown in Fig. 6, all the samples exhibited a broad emission peak centered around 450 nm, which can be attributed to the band–band PL phenomenon with the light energy approximately equal to the band gap energy of g-C_3N_4. The lower PL emission peak intensity for CN-450 was attributed to the rich-defected heterocycle formed from incomplete condensation. The PL intensity decreased with increasing the polymeric temperature from 500 to 600 °C, which indicates a suppressed recombination rate of the photo-induced charge carriers. The main benefit derives from the optimized construction of the layer stacking structure, which hastens the mobility of the free charge carriers and facilitates a high photocatalytic rate.

In addition, room-temperature EPR analysis was carried out to investigate the electronic band structure of the porous g-C_3N_4 samples. In Fig. 7, one single Lorentzian line, centered at a g value of 2.0034 originating from the unpaired electrons in the aromatic rings of carbon atoms, is observed for all of the g-C_3N_4 samples.

For samples obtained under a gradually increasing temperature, the enhanced spectral line intensity of EPR, demonstrates the progressive development of the electronic band structure. A larger surface area is a key factor for the enhancement of the EPR Lorentzian line, therefore, increasing the density of the surface sites of the catalysts [34].

3.2. Photocatalytic performance

The visible light photocatalytic activity of CN-*T* samples for H_2 evolution was evaluated in an aqueous proton solution under visible light irradiation (λ > 420 nm). Chloroplatinic acid (Pt nanoparticles) and triethanolamine were used as co-catalyst and electron donors, respectively. The H_2 evolution rates (HER) for samples obtained at different temperatures are shown in Fig. 8(a). We observe that treatment at a higher

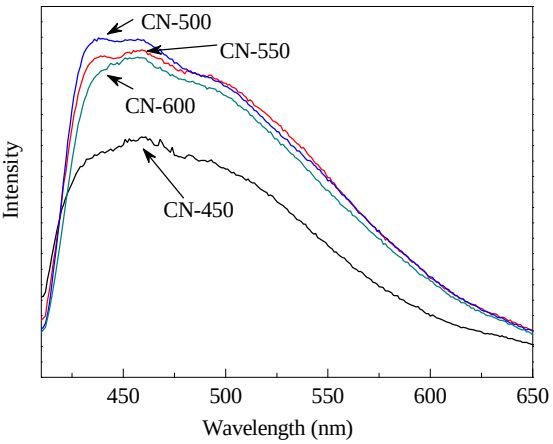

Fig. 6. PL spectra of the CN samples.

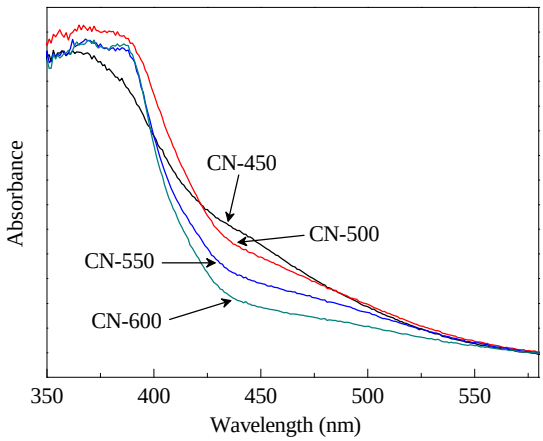

Fig. 5. UV-vis DRS spectra of the CN samples.

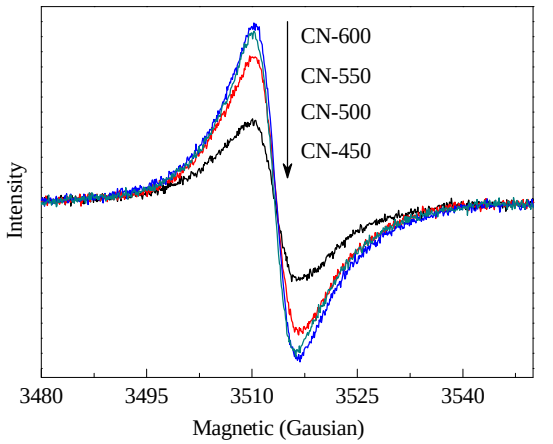

Fig. 7. EPR signals of the CN samples.

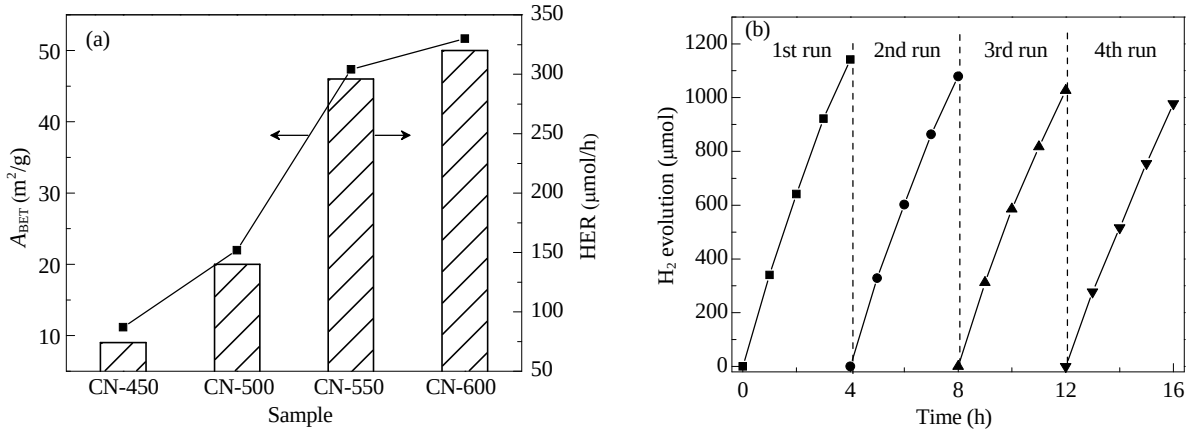

Fig. 8. (a) The correlation between A_{BET} and the H_2 evolution rate for CN samples. (b) Time course of H_2 evolution for CN-600 under visible light irradiation (λ > 420 nm).

temperature is beneficial for the photocatalytic activity of the CN catalyst. The HER of CN-600 reaches 340 μmol/h, nearly 2.2 times that of CN-500. In addition, the HER of the obtained CN samples obeys a direct correlation with the corresponding surface area. A 16-h recycling experiment with intermittent evacuation every 4 h was performed on CN-600 under visible light (λ > 420 nm), and acceptable (photo)-chemical stability of CN could be obtained.

Compared with the previously prepared CN nanosheets through various methods, the enlarged surface area of our prepared porous g-C_3N_4 nanosheets is not conspicuous. However, the HER of CN samples obtained in ammonia condensation on each unit of their specific surface area was greatly improved. Hence, in addition to the introduction of a porous structure, the improved polymerization degree of materials plays a significant role in the photocatalytic H_2 evolution activity. The conclusion can be derived that the novel g-C_3N_4 material with improved polymerization degree and nanopores exhibits excellent photocatalytic activity and stability for H_2 evolution.

4. Conclusions

Porous g-C_3N_4 nanosheets were successfully prepared through a one-step ammonia thermopolymerization method at high temperatures. The inhibitory effect of ammonia from NH_4SCN decomposition under high temperature optimizes the polymeric layer structure of the g-C_3N_4 nanosheet. The higher condensation temperature results in more nanopores, larger surface area, wider bandgap and a lower recombination rate of photo-induced carriers in the samples, thereby improving the photocatalytic activity for H_2 evolution under visible light irradiation. This route for the preparation of 2D porous CN-based polymer semiconductors nanosheets is easily-conducted, and the physicochemical properties of the samples are conveniently designed and adjusted.

References

[1] X. F. Song, J. L. Hu, H. B. Zeng, *J. Mater. Chem. C*, **2013**, 1, 2952–2969.
[2] K. Dolui, C. D. Pemmaraju, S. Sanvito, *ACS Nano*, **2012**, 6, 4823–4834.
[3] Y. Lin, J. W. Connell, *Nanoscale*, **2012**, 4, 6908–6939.
[4] J. H. Xiong, Y. H. Liu, D. K. Wang, S. J. Liang, W. M. Wu, L. Wu, *J. Mater. Chem. A*, **2015**, 3, 12631–12635.
[5] B. Mahler, V. Hoepfner, K. Liao, G. A. Ozin, *J. Am. Chem. Soc.*, **2014**, 136, 14121–14127.
[6] Y. F. Sun, Z. H. Sun, S. Gao, H. Cheng, Q. H. Liu, J. Y. Piao, T. Yao, C. Z. Wu, S. L. Hu, S. Q. Wei, Y. Xie, *Nat. Commun.*, **2012**, 3, 1057–1063.
[7] K. M. Cho, K. H. Kim, H. O. Choi, H. T. Jung, *Green Chem.*, **2015**, 17, 3972–3978.
[8] M. Z. Rahman, C. W. Kwong, K. Davey, S. Z. Qiao, *Energy Environ. Sci.*, **2016**, 9, 709–728.
[9] Y. Zheng, J. Liu, J. Liang, M. Jaroniecc, S. Z. Qiao, *Energy Environ. Sci.*, **2012**, 5, 6717–6731.
[10] Y. J. Cui, *Chin. J. Catal.*, **2015**, 36, 372–379.
[11] Q. Han, B. Wang, Y. Zhao, C. G. Hu, L. T. Qu, *Angew. Chem. Int. Ed.*, **2015**, 54, 11433–11437.
[12] Z. Z. Lin, X. C. Wang, *Angew. Chem. Int. Ed.*, **2013**, 52, 1735–1738.
[13] J. S. Zhang, Y. Chen, X. C. Wang, *Energy Environ. Sci.*, **2015**, 8, 3092–3108.
[14] Y. Zheng, L. H. Lin, B. Wang, X. C. Wang, *Angew. Chem. Int. Ed.*, **2015**, 54, 12868–12884.
[15] X. D. Zhang, X. Xie, H. Wang, J. J. Zhang, B. K. Pan, Y. Xie, *J. Am. Chem. Soc.*, **2013**, 135, 18–21.
[16] Q. Y. Lin, L. Li, S. J. Liang, M. H. Liu, J. H. Bi, L. Wu, *Appl. Catal. B*, **2015**, 163, 135–142.
[17] L. S. Lin, Z. X. Cong, J. Li, K. M. Ke, S. S. Guo, H. H. Yang, G. N. Chen, *J. Mater. Chem. B*, **2014**, 2, 1031–1037.
[18] J. Xu, L. W. Zhang, R. Shi, Y. F. Zhu, *J. Mater. Chem. A*, **2013**, 1, 14766–14772.
[19] S. Y. Deng, P. X. Yuan, X. B. Ji, D. Shan, X. J. Zhang, *ACS Appl. Mater. Interfaces*, **2015**, 7, 543–552.
[20] H. Xu, J. Yan, X. J. She, L. Xu, J. X. Xia, Y. G. Xu, Y. H. Song, L. Y. Huang, H. M. Li, *Nanoscale*, **2014**, 6, 1406–1415.
[21] Y. Yin, J. C. Han, X. H. Zhang, Y. M. Zhang, J. G. Zhou, D. Muir, R. Sutarto, Z. H. Zhang, S. W. Liu, B. Song, *RSC Adv.*, **2014**, 4, 32690–32697.
[22] F. X. Cheng, H. N. Wang, X. P. Dong, *Chem. Commun.*, **2015**, 51, 7176–7179.
[23] Q. J. Lu, J. H. Deng, Y. X. Hou, H. Y. Wang, H. T. Li, Y. Y. Zhang, *Chem. Commun.*, **2015**, 51, 12251–12253.

Graphical Abstract

Chin. J. Catal., 2016, 37: 1899–1906 doi: 10.1016/S1872-2067(16)62509-3

Polycondensation of ammonium thiocyanate into novel porous g-C_3N_4 nanosheets as photocatalysts for enhanced hydrogen evolution under visible light irradiation

Yanjuan Cui *, Yuxiong Wang, Hao Wang, Fu Cao, Fangyan Chen
Jiangsu University of Science and Technology

Polymer semiconductor g-C_3N_4 nanosheets with abundant pores synthesized from a one-step ammonia thermopolymerization method are demonstrated as a stable photocatalyst for H_2 evolution under visible light irradiation.

[24] P. Niu, L. L. Zhang, G. Liu, H. M. Cheng, *Adv. Funct. Mater.*, **2012**, 22, 4763–4770.
[25] F. Dong, Y. H. Li, Z. Y. Wang, W. K. Ho, *Appl. Surf. Sci.*, **2015**, 358, 393–403.
[26] J. J. Zhu, P. Xiao, H. L. Li, S. A. C. Carabineiro, *ACS Appl. Mater. Interfaces*, **2014**, 6, 16449–16465.
[27] Y. J. Cui, J. H. Huang, X. Z. Fu, X. C. Wang, *Catal. Sci. Technol.*, **2012**, 2, 1396–1402.
[28] J. H. Huang, M. Antonietti, J. Liu, *J. Mater. Chem. A*, **2014**, 2, 7686–7693.
[29] Q. J. Fan, J. J. Liu, Y. C. Yu, S. L. Zuo, *RSC Adv.*, **2014**, 4, 61877–61883.
[30] M. Zhang, J. Xu, R. L. Zong, Y. F. Zhu, *Appl. Catal. B*, **2014**, 147, 229–235.
[31] J. C. Shen, H. Yang, Q. H. Shen, Y. Feng, Q. F. Cai, H. Y. Yang, *Eur. J. Inorg. Chem.*, **2015**, 15, 2611–2618.
[32] Y. J. Cui, G. G. Zhang, Z. Z. Lin, X. C. Wang, *Appl. Catal. B*, **2016**, 181, 413–419.
[33] Y. Q. Cao, Z. Z. Zhang, J. L. Long, J. Liang, H. Lin, H. X. Lin, X. X. Wang, *J. Mater. Chem. A*, **2014**, 2, 17797–17807.
[34] G. G. Zhang, J. S. Zhang, M. W. Zhang, X. C. Wang, *J. Mater. Chem.*, **2012**, 22, 8083–8091.

热聚合硫氰酸铵制备多孔 g-C_3N_4 纳米片及其可见光催化分解水制氢性能

崔言娟*, 王愉雄, 王 浩, 曹 福, 陈芳艳
江苏科技大学环境与化学工程学院, 江苏镇江 212003

摘要: 二维层状半导体材料与其体相堆积结构相比表现出独特的性质, 有望在纳米材料科学领域取得新的突破. 基于对太阳能利用的研究, 二维半导体光催化材料引起了研究者的广泛关注. 诸多半导体材料已被设计合成二维纳米片结构应用于光催化领域, 如 MoS_2, WS_2, SnS_2和TiO_2 等. 石墨相氮化碳 (g-C_3N_4) 是一种典型的非金属二维聚合物半导体. 二维层状结构的组成使得 g-C_3N_4 纳米片能够表现出优异的光电性质. 然而, 其合成目前仍然存在很大困难. 目前已报道的单层或多层 g-C_3N_4 的制备主要有超声辅助溶剂剥离法、热处理法、插层法和电化学合成法等. 但这些方法存在合成复杂和引入结构缺陷等不足. 另外, 在体相组成中插入孔结构也能够提高 g-C_3N_4 的光催化活性. 目前常用的方法主要是模板法. 然而, 在这些生孔过程中往往引起聚合度降低, 增加长程无序度, 不利于光生载流子的传输. 因此, 如果将多孔结构引入 g-C_3N_4 纳米片, 同时提高其聚合度结构, 将在很大程度上提高其光催化性能.

本文利用直接氨气热聚合的方法, 将硫氰酸铵进行高温热处理, 一步法合成出较高聚合度的多孔 g-C_3N_4 纳米片, 在可见光照射下表现出较高的产氢活性和稳定性. 采用 X射线衍射 (XRD)、红外光谱 (FTIR)、荧光光谱 (PL)和电子顺磁共振 (EPR) 等方法对多孔 g-C_3N_4 纳米片结构进行了详细表征. 在助催化剂 Pt 存在下, 采用可见光照射 (> 420 nm) 分解水产氢的方法评价了其光催化性能.

结果表明, 热处理温度对产物结构及性能具有较大影响. XRD 结果表明, 在 450 °C 热处理, 硫氰酸铵未完全聚合, 与前期氮气热处理的结论不同. 当热聚合温度上升至 500 °C, 石墨相结构形成. 至 600 °C 时, 石墨相的层间距缩小, 且聚合度没有明显下降. 这表明氨气气氛抑制了原料分解, 提高了分解聚合温度, 同时增加了产物的聚合度. FTIR 结果表明, 热聚合温度对产物 C–N 共轭结构改变不大, 但在 810 cm^{-1} 处的峰位向长波数移动, 表明七嗪环单元含量增加, 再次证明高的热聚合温度没有造成明显的结构分解, 反而促进了聚合结构的形成. 扫描电镜与氮气吸脱附分析表明, 随着聚合温度升高, 产

物粒子尺寸变小, 形貌呈现层状分布, 并伴随多孔状的产生, 因此比表面积和孔体积显著增大, 吸收带边发生蓝移. PL 和 EPR 结果表明, 聚合温度从 500 增至 600 ºC, 样品光生载流子的复合速率下降, 导带离域电子密度增加, 从而有利于光催化性能的提高. 光解水产氢性能测试表明, 聚合温度升高有利于催化剂产氢速率提高; 600 ºC 所得样品的产氢速率达 340 μmol/h. 进一步分析表明, 产氢速率与比表面积基本成正相关关系, 说明层状多孔结构的形成是影响产氢性能的重要因素. 经过多轮循环测试, 其产氢性能保持稳定而没有显著下降, 表明其活性稳定性良好.

关键词: 氮化碳; 纳米片; 半导体; 氨; 光催化; 产氢

收稿日期: 2016-05-11. 接受日期: 2016-07-18. 出版日期: 2016-11-05.

*通讯联系人. 电话/传真: (0511)85605157; 电子信箱: yjcui@just.edu.cn

基金来源: 国家自然科学基金 (21503096); 江苏省自然科学基金 (BK20140507).

本文的英文电子版由Elsevier出版社在ScienceDirect上出版(http://www.sciencedirect.com/science/journal/18722067).